International Journal of Heat and Mass Transfer 58 (2013) 229–239

Contents lists available at SciVerse ScienceDirect

International Journal of Heat and Mass Transfer

journal homepage: www.elsevier.com/locate/ijhmt

Thermal analysis of microwave assisted bonding of poly(methyl methacrylate) substrates in microfluidic devices

Kasi Balamurugan Mani, Mohammad Robiul Hossan, Prashanta Dutta *

School of Mechanical and Materials Engineering, Washington State University, Pullman, WA 99164-2920, United States

ARTICLE INFO

Article history:
Received 21 May 2012
Received in revised form 1 November 2012
Accepted 6 November 2012

Keywords:
Microwave heating
Multilayer
Polymer bonding
PMMA
Poly-aniline

ABSTRACT

Electromagnetic heating such as microwave processing has evolved as a promising technique to bond polymer substrates due to its ability to achieve non-contact, selective heating and localized melting. In microwave assisted bonding process, two polymer layers such as PMMA (polymethyl methacrylate) substrates can be bonded by heating a thin layer of dielectric material placed between the polymer layers. To better understand the bonding process of polymer layers, a detailed theoretical analysis has been presented. In this analysis, the bonding process of polymer substrates has been modeled as a multilayered composite slab exposed to microwave radiations. The electric field distribution along each layer is computed from simplified Maxwell's equation under plane wave configuration, and the Poynting theorem is used to find the volumetric power absorbed by each layer. The absorbed power is then used as the source term in unsteady energy equation which is solved by linear decomposition and separation of variables techniques. Finally, the closed form analytical solution obtained from this analysis is used to study the effect of material properties on temperature distribution of polymer substrate (PMMA) with poly-aniline as intermediate sacrificial layer. The analysis was carried out at household microwave frequency (2.4 GHz) with temperature dependent dielectric properties for both poly-aniline and PMMA layers. Our results show that dielectric properties, layer thickness, heat transfer coefficient and processing time have significant influence on the heating pattern. Results also show that the temperature of the PMMA substrate remains below the melting point globally, except at the interface of the poly-aniline layer due to its transparent nature to incident microwave radiation at 2.4 GHz.

1. Introduction

Microfluidic devices are finding numerous applications in areas such as analytical chemistry, microbiology, drug development and chemical synthesis [1–7]. These devices have many advantages such as compact size, disposability, increased functionality and reliability, reduced analysis time and accuracy. In microfluidic devices, glass substrates have been used as the preferred material of choice due to its low cost. However, fabrication process for glass microdevice is very challenging especially for complex device. Moreover, optical characteristics of glass substrates are not suitable for many lab-on-a-chip devices [8]. In recent years, polymers are found to effectively replace glass as substrate materials in microfluidic device fabrication. Polymers possess wide range of physical and chemical properties suitable for chemical and biological analysis, offer low manufacturing cost, provide good optical clarity etc. Different polymers such as polydimethylsiloxane (PDMS), polymethyl methacrylate (PMMA), cyclic olefin copolymer (COC), polycarbonates (PC) are widely used for microfluidic device fabrication [9,10].

In microfabrication process the polymer substrates, with or without patterned micro feature, need to be bonded to effectively make a functional microchannel. The bonding process is a very challenging issue as it should be carried out without changing or destroying the integrity of the patterned microstructure. Bonding techniques such as adhesive bonding, thermal bonding, solvent bonding and resin-gas injection bonding have been reported in the literatures [11–14]. However, these techniques either cause geometric deformation of the substrate or induce a chemical reaction that affects the patterned micro channel. Therefore, it is necessary to develop an alternative technique to bond polymer based microfluidic devices.

Recently, the use of microwave technology has been reported to achieve bonding, and it has been found that this technique is especially very effective for bonding PMMA substrates in microfluidic devices without causing any change or destruction to the patterned microstructures [15–19]. In microwave assisted bonding, a very thin layer of dielectric material is placed between two layers of PMMA as shown in Fig. 1, and the ability of material selective

* Corresponding author. Tel.: +1 (509) 335 7989; fax: +1 (509) 335 4662.
E-mail address: dutta@mail.wsu.edu (P. Dutta).

0017-9310/$ - see front matter © 2012 Elsevier Ltd. All rights reserved.
http://dx.doi.org/10.1016/j.ijheatmasstransfer.2012.11.010

Nomenclature

A_n	coefficient for nth layer [V/m]
B_n	coefficient for nth layer [V/m]
$\vec{B}$	magnetic induction [Wb/m^2]
c	velocity of light [m/s]
C_p	specific heat capacity [J/kg K]
$\vec{D}$	electric displacement [C/m^2]
$\vec{E}$	electric field [V/m]
E_o	impinging electromagnetic field [V/m]
E_x	electric field in x direction [V/m]
E_y	electric field in y direction [V/m]
E_z	electric field in z direction [V/m]
$E_{z,n}$	electric field in z direction for nth layer [V/m]
$E_{z,0}$	electric field in z direction in air medium [V/m]
F_n	initial condition for nth layer [°C]
$\overline{F}_n$	modified initial condition for nth layer [°C]
f	frequency [Hz]
G	Green's function
$\vec{H}$	magnetic field [A/m]
H_y	magnetic field in y direction [A/m]
$H_{y,n}$	magnetic field in y direction for nth layer [A/m]
h	heat transfer coefficient [W/m^2 K]
I	incident microwave energy flux [W/cm^2]
$\vec{J}$	current density [A/m^2]
k_n	thermal conductivity for nth layer [W/m K]
L_n	thickness of nth layer [m]
$\vec{P}$	Poynting power flux vector [W/m^2]
P_{abs}	power absorbed by the layer [W]
$P_{incident}$	total incident power [W]
$\dot{Q}$	power generation [W/m^3]
$\dot{Q}_n$	power generation for nth solid layer[W/m^3]
$R_{n,n+1}$	reflection coefficient
T_n	temperature for nth layer [°C]
T_a,T_b	surrounding temperature [°C]
Δt	time step [s]
t_{total}	total duration of electromagnetic heating [s]
$T_{n,n+1}$	transmission coefficient for wave travelling towards positive x axis
$T_{n+1,n}$	transmission coefficient for wave travelling towards negative x axis
X_n	modified temperature for nth layer [°C]
x	location along x coordinate [m]
y	location along y coordinate [m]
z	location along z coordinate [m]

Greek symbols

α_n	thermal diffusivity for nth layer [m^2/s]
β_n	phase factor for nth layer [rad/m]
γ	propagation constant [m^{-1}]
γ_n	propagation constant for nth layer [m^{-1}]
δ_n	dissipation factor for nth layer [rad]
ε	permittivity [F/m]
ε_0	free-space permittivity [F/m]
ε_r	relative permittivity [dimensionless]
ε'_n	relative dielectric constant for nth layer [dimensionless]
ε''_n	relative dielectric loss for nth layer [dimensionless]
λ_m	eigenvalues in the x-direction
μ	permeability [H/m]
μ_0	free-space permeability [H/m]
ϕ_n	modified temperature for nth layer [°C]
ψ_n	modified temperature for nth layer [°C]
θ_n	modified temperature for nth layer [°C]
Γ_n	modified temperature for nth layer [°C]
ρ	mass density [kg/m^3]
ρ_v	charge density [C/m^3]
τ	modified time for Green's function [s]
σ_n	attenuation constant [rad/m]
σ'	electrical conductivity [S/m]
ζ	impedance [ohm]
ω	angular frequency [rad/s]

Subscripts

j	layer index
m	eigenvalue index
n	layer index

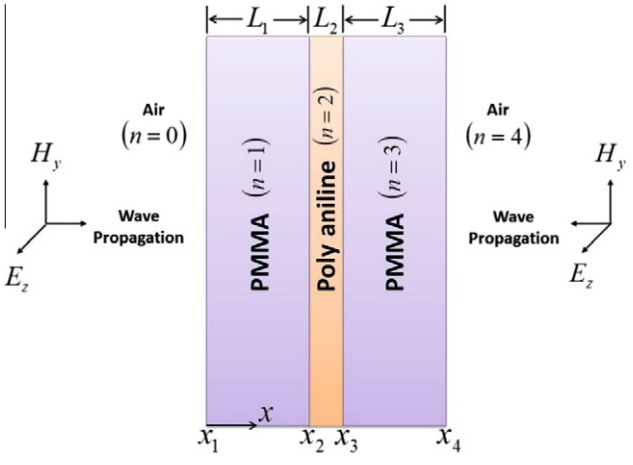

Fig. 1. Schematic of a three layered object exposed to a plane electromagnetic wave. In a uniform plane wave, the magnetic field is always perpendicular to the electric field. The thickness of each layer is denoted as L_1,L_2,L_3 and the locations of the interface are presented as x_1,x_2,x_3, and x_4. The value for ***n*** in each layer denotes the layer number.

heat generation resulted from microwave radiation is used for bonding purpose. Since PMMA layers are transparent to microwave radiation, the temperature rise in PMMA is not as high as in the sandwiched dielectric layer. This high temperature at the interface results in a localized melting of the PMMA substrates which is the main reason for irreversible bonding of PMMA layers.

The microwave bonding of PMMA microfluidic devices using highly dielectric materials such as ethanol, methanol and isopropyl alcohol as a thin sacrificial layer were examined experimentally [17]. Recently, polymers such as poly-aniline and polythiophene have evolved as a new class of sacrificial materials for PMMA bonding. However, the amount of sacrificial material required for effective bonding of the PMMA substrate has been a major issue and requires fundamental understanding for perfect bonding [16,18]. For instance, bonding would be very weak, if the thickness of the sacrificial layer is less than optimum. On the other hand, there will be significant distortion of the channel feature if the thickness of the interfacial sacrifice layer is very thick. Also microwave exposure time and intensity are very crucial for successful bonding process. Yussuf et al. [16] experimented with poly-aniline to bond PMMA substrates under microwave power and found to achieve strong bonding at the interface that could withstand a pressure up to 1.18 MPa. Lately, Holmes et al. [19] experimented with varying widths and depths of the poly-aniline layer to bond PMMA substrates for defect free seals.

Although there are numerous experimental studies on the use of sacrificial layer for bonding PMMA substrates using microwave radiation, no theoretical study has been reported to understand the fundamental mechanism of PMMA–PMMA bonding. A detail thermal analysis can reveal the local temperature distribution within materials as a function of time, which can explain the microwave assisted bonding process. Moreover, a theoretical analysis can provide the desired correlation between the characteristics of electromagnetic wave and geometric, dielectric, and thermo-physical properties of materials subjected to microwave heating.

The rest of the paper is organized as follows. First the theory and governing equations for electromagnetic heating are provided followed by underlying assumptions for this analytic study. Then an analysis to find the electromagnetic heat generation is presented for each layer. Next, the temperature distribution within each layer is obtained from the energy equation using linear decomposition and separation of variables techniques. This is followed by a discussion on polymer bonding by analyzing the temperature distribution in PMMA and poly-aniline materials at various times for different thicknesses of poly-aniline and PMMA. Finally, we present our conclusions on this analytic work.

2. Theory

Microwave heating is generally very effective for dielectric materials which contains either permanent or induced dipoles. When electromagnetic radiation with alternating electric field is applied across the dielectric material, the positive and negative charges of the dipole get aligned towards the electric field and result in polarization of the medium. Due to the alternating nature of electric field, dipoles rotate as they try to align with the electric field of the incident electromagnetic radiation. The rotation of dipoles results in heat generation inside the dielectric material. Therefore, to study the microwave heating it is necessary to understand the electromagnetic field within the dielectric material as well as its effects in energy equation.

2.1. Governing equations

The electromagnetic field distribution within a material is governed by Maxwell's equation as [20,21].

$$\vec{\nabla}\times\vec{E}=-\frac{\partial\vec{B}}{\partial t} \tag{1a}$$

$$\vec{\nabla}\times\vec{H}=\vec{J}+\frac{\partial\vec{D}}{\partial t} \tag{1b}$$

$$\vec{\nabla}\cdot\vec{D}=\rho_v \tag{1c}$$

$$\vec{\nabla}\cdot\vec{B}=0 \tag{1d}$$

where $\vec{E}$ is the electric field, $\vec{B}$ is the magnetic induction, $\vec{H}$ is the magnetic field, $\vec{J}$ is the current density, $\vec{D}$ is the electric displacement, and ρ_v is the electric charge density. The time averaged power flux associated with the electromagnetic wave can be obtained from Poynting vector [21]

$$\vec{P}=\frac{1}{2}(\vec{E}\times\vec{H}^*) \tag{2a}$$

where $\vec{H}^*$ is the complex conjugate of magnetic field. The volumetric heat generation can be obtained as

$$\dot{Q}=Re(-\vec{\nabla}\cdot\vec{P}) \tag{2b}$$

For electromagnetic heating, the temperature distribution within the system is governed by the energy equation as [25]:

$$\rho C_p\frac{dT}{dt}=\vec{\nabla}\cdot(k\vec{\nabla}T)+\dot{Q} \tag{3}$$

The left hand side term represents the rate of thermal energy change in the system, while the first term in the right hand side accounts for the thermal diffusion.

2.2. Assumptions

In this study, we assume that the thickness of each layer is much smaller compared to the other (length and width) dimensions and hence one-dimensional analysis of the system, as shown in Fig. 1, is reasonable for microwave assisted bonding of two PMMA layers using poly-aniline as sacrificial layer. For simplicity, we assume that electromagnetic waves are transverse (TEM) or uniform plane waves. The other assumptions used to simplify the problem are:

(i) Multilayered system obeys linear material constitutive laws.
(ii) Electroneutrality condition is satisfied within the system.
(iii) The magnetic permeability $\mu(\omega)$ can be approximated by its value in free space.
(iv) Dielectric properties are assumed to be temperature independent for a short duration of processing time.
(v) Material properties such as thermal conductivity and specific heat of each solid are temperature independent.
(vi) Perfect thermal contact exists at the layer interface.
(vii) The surrounding medium (air) is at ambient temperature.

Similar assumptions are used in earlier theoretical studies of electromagnetic heating [21–24].

3. Analysis

3.1. Electromagnetic power

Maxwell's equations can be simplified by using the assumptions mentioned above and by applying following material constitutive relations [25]

$$\vec{J}=\sigma'\vec{E} \tag{4a}$$

$$\vec{D}=\varepsilon\vec{E} \tag{4b}$$

$$\vec{B}=\mu\vec{H} \tag{4c}$$

where σ' is the electrical conductivity, ε is the permittivity, and μ is the magnetic permeability. The expression for permittivity can be written as [20]:

$$\left.\begin{aligned}\varepsilon&=\varepsilon_0\varepsilon_r\\ \varepsilon_r&=\varepsilon'-i\varepsilon''\end{aligned}\right\} \tag{5}$$

If electromagnetic incident rays are propagating in the x-direction (Fig. 1), then

$$E_x=E_y=0 \tag{6a}$$

$$\frac{\partial E_z}{\partial y}=\frac{\partial E_z}{\partial z}=0 \tag{6b}$$

Therefore, for a uniform plane wave, the simplified equation for electric field can be written as:

$$\frac{d^2E_z}{dx^2}-\gamma^2E_z=0 \tag{7}$$

In a multilayered system, the electric field for the nth layer is obtained by modifying Eq. (7) as,

$$\frac{d^2E_{z,n}}{dx^2}-\gamma_n^2E_{z,n}=0\quad\text{in } x_n\leqslant x\leqslant x_{n+1},\ n=1,\ldots,3 \tag{8}$$

where γ_n is the propagation constant, and it can be given as $\gamma_n^2 = -\omega^2\mu_0\varepsilon_0(\varepsilon'_n - i\varepsilon''_n)$. The propagation constant can also be expressed as $\gamma_n = \sigma_n + i\beta_n$, where the attenuation factor and the phase factor can be given by Eqs. (9a) and (9b), respectively.

$$\sigma_n = \frac{2\pi f}{c}\sqrt{\frac{\varepsilon'_n\left(\sqrt{1+\tan^2\delta_n}-1\right)}{2}} \tag{9a}$$

$$\beta_n = \frac{2\pi f}{c}\sqrt{\frac{\varepsilon'_n\left(\sqrt{1+\tan^2\delta_n}+1\right)}{2}} \tag{9b}$$

where $\tan\delta_n = \frac{\varepsilon''_n}{\varepsilon'_n}$ is the dissipation factor.

For a uniform plane electromagnetic wave propagating in the x direction of a multilayered sample (Fig. 1), the boundary conditions and interface conditions are given by

$$\left.\begin{aligned} E_{z,0} &= E_{z,1} \\ \tfrac{dE_{z,0}}{dx} &= \tfrac{dE_{z,1}}{dx} \end{aligned}\right\} \quad \text{at } x = x_1 \tag{10a}$$

$$\left.\begin{aligned} E_{z,n}\big|_{x=x_{n+1}} &= E_{z,n+1}\big|_{x=x_{n+1}} \\ \left.\tfrac{dE_{z,n}}{dx}\right|_{x=x_{n+1}} &= \left.\tfrac{dE_{z,n+1}}{dx}\right|_{x=x_{n+1}} \end{aligned}\right\}, \quad n = 1,\ldots,2 \tag{10b}$$

$$\left.\begin{aligned} E_{z,3} &= E_{z,4} \\ \tfrac{dE_{z,3}}{dx} &= \tfrac{dE_{z,4}}{dx} \end{aligned}\right\} \quad \text{at } x = x_4 \tag{10c}$$

where subscripts 0 and 4 denotes the electric and magnetic field surrounding air. The generalized solution for simplified Maxwell's equation for multilayered materials can be expressed as:

$$E_{z,n} = A_n e^{-\gamma_n x} + B_n e^{\gamma_n x} \quad \text{in } x_n \leqslant x \leqslant x_{n+1},\ n = 1,\ldots,3 \tag{11}$$

Applying the boundary conditions (10a)–(10c) in the general solution (11), the coefficients A_n and B_n for each layer of solid can be found as,

$$A_1 = \frac{E_0 e^{x_2\gamma_1}\left[T_{0,1}e^{L_1\gamma_1}\left(R_{1,2}R_{2,3}e^{2L_3\gamma_3} + R_{3,4}R_{1,2} + R_{3,4}R_{2,3}e^{2L_2\gamma_2} + e^{2(L_2\gamma_2+L_3\gamma_3)}\right) - T_{2,1}T_{3,2}T_{0,3}R_{0,1}e^{(L_2\gamma_2+L_3\gamma_3)}\right]}{e^{2(L_1\gamma_1+L_2\gamma_2+L_3\gamma_3)} + R_{0,1}R_{3,4} + R_{0,1}R_{1,2}e^{2L_2\gamma_2}\left(e^{2L_3\gamma_3}+R_{3,4}R_{2,3}\right) + R_{2,3}e^{2L_3\gamma_3}\left(e^{2L_1\gamma_1}R_{1,2}+R_{0,1}\right) - e^{2L_1\gamma_1}R_{3,4}\left(e^{2L_2\gamma_2}R_{2,3}+R_{1,2}\right)} \tag{12a}$$

$$B_1 = \frac{E_0 e^{-x_1\gamma_1}e^{L_1\gamma_1}\left[T_{0,1}e^{-L_1\gamma_1}\left(R_{3,4}R_{1,2}R_{2,3}e^{2L_2\gamma_2} + R_{3,4} + R_{2,3}e^{2L_3\gamma_3} + R_{1,2}e^{2(L_2\gamma_2+L_3\gamma_3)}\right) + T_{3,2}T_{2,1}T_{0,3}e^{(L_2\gamma_2+L_3\gamma_3)}\right]}{e^{2(L_1\gamma_1+L_2\gamma_2+L_3\gamma_3)} + R_{0,1}R_{3,4} + R_{0,1}R_{1,2}e^{2L_2\gamma_2}\left(e^{2L_3\gamma_3}+R_{3,4}R_{2,3}\right) + R_{2,3}e^{2L_3\gamma_3}\left(e^{2L_1\gamma_1}R_{1,2}+R_{0,1}\right) - e^{2L_1\gamma_1}R_{3,4}\left(e^{2L_2\gamma_2}R_{2,3}+R_{1,2}\right)} \tag{12b}$$

$$A_2 = \frac{E_0 e^{x_3\gamma_2}e^{L_2\gamma_2}\left[T_{0,1}T_{1,2}e^{L_1\gamma_1}\left(R_{3,4}R_{2,3}+e^{2L_3\gamma_3}\right) - T_{3,2}T_{0,3}e^{(L_3\gamma_3-L_2\gamma_2)}\left(R_{0,1}+R_{1,2}e^{2L_1\gamma_1}\right)\right]}{e^{2(L_1\gamma_1+L_2\gamma_2+L_3\gamma_3)} + R_{0,1}R_{3,4} + R_{0,1}R_{1,2}e^{2L_2\gamma_2}\left(e^{2L_3\gamma_3}+R_{3,4}R_{2,3}\right) + R_{2,3}e^{2L_3\gamma_3}\left(e^{2L_1\gamma_1}R_{1,2}+R_{0,1}\right) - e^{2L_1\gamma_1}R_{3,4}\left(e^{2L_2\gamma_2}R_{2,3}+R_{1,2}\right)} \tag{12c}$$

$$B_2 = \frac{E_0 e^{-x_2\gamma_2}e^{L_2\gamma_2}\left[T_{3,2}T_{0,3}e^{L_3\gamma_3}\left(R_{0,1}R_{1,2}+e^{2L_1\gamma_1}\right) + T_{1,2}T_{0,1}e^{(L_1\gamma_1-L_2\gamma_2)}\left(R_{3,4}+R_{2,3}e^{2L_3\gamma_3}\right)\right]}{e^{2(L_1\gamma_1+L_2\gamma_2+L_3\gamma_3)} + R_{0,1}R_{3,4} + R_{0,1}R_{1,2}e^{2L_2\gamma_2}\left(e^{2L_3\gamma_3}+R_{3,4}R_{2,3}\right) + R_{2,3}e^{2L_3\gamma_3}\left(e^{2L_1\gamma_1}R_{1,2}+R_{0,1}\right) - e^{2L_1\gamma_1}R_{3,4}\left(e^{2L_2\gamma_2}R_{2,3}+R_{1,2}\right)} \tag{12d}$$

$$A_3 = \frac{E_0 e^{x_3\gamma_3}e^{L_3\gamma_3}\left[T_{0,1}T_{1,2}T_{2,3}e^{L_1\gamma_1+L_2\gamma_2+L_3\gamma_3} - T_{0,3}R_{0,1}R_{1,2}R_{2,3}e^{2L_2\gamma_2} - T_{0,3}R_{0,1} - T_{0,3}R_{1,2}e^{2L_1\gamma_1} - T_{0,3}R_{2,3}e^{2(L_1\gamma_1+L_2\gamma_2)}\right]}{e^{2(L_1\gamma_1+L_2\gamma_2+L_3\gamma_3)} + R_{0,1}R_{3,4} + R_{0,1}R_{1,2}e^{2L_2\gamma_2}\left(e^{2L_3\gamma_3}+R_{3,4}R_{2,3}\right) + R_{2,3}e^{2L_3\gamma_3}\left(e^{2L_1\gamma_1}R_{1,2}+R_{0,1}\right) - e^{2L_1\gamma_1}R_{3,4}\left(e^{2L_2\gamma_2}R_{2,3}+R_{1,2}\right)} \tag{12e}$$

$$B_3 = \frac{E_0 e^{-x_3\gamma_3}e^{L_3\gamma_3}\left[T_{0,3}R_{0,1}R_{2,3} + T_{0,3}R_{0,1}R_{1,2}e^{2L_2\gamma_2} + T_{0,3}R_{1,2}R_{2,3}e^{2L_1\gamma_1} + T_{0,3}e^{2(L_1\gamma_1+L_2\gamma_2)} + T_{2,3}T_{0,1}T_{1,2}R_{3,4}e^{L_1\gamma_1+L_2\gamma_2-L_3\gamma_3}\right]}{e^{2(L_1\gamma_1+L_2\gamma_2+L_3\gamma_3)} + R_{0,1}R_{3,4} + R_{0,1}R_{1,2}e^{2L_2\gamma_2}\left(e^{2L_3\gamma_3}+R_{3,4}R_{2,3}\right) + R_{2,3}e^{2L_3\gamma_3}\left(e^{2L_1\gamma_1}R_{1,2}+R_{0,1}\right) - e^{2L_1\gamma_1}R_{3,4}\left(e^{2L_2\gamma_2}R_{2,3}+R_{1,2}\right)} \tag{12f}$$

where the transmission coefficients,

$$\left.\begin{aligned} T_{n,n+1} &= \tfrac{2\zeta_{n+1}}{\zeta_{n+1}+\zeta_n} \\ T_{n+1,n} &= \tfrac{2\zeta_n}{\zeta_{n+1}+\zeta_n} \end{aligned}\right\}, \quad n = 0,\ldots,3 \tag{13a}$$

the reflection coefficient,

$$R_{n,n+1} = \frac{\zeta_{n+1}-\zeta_n}{\zeta_{n+1}+\zeta_n}, \quad n = 0,\ldots,3 \tag{13b}$$

and the intrinsic impedance $\zeta = \sqrt{\frac{\mu}{\varepsilon}}$, [24]. Once the electric field distribution is known, the magnetic field distribution can be evaluated easily as they are related by,

$$\frac{dE_{z,n}}{dx} = -i\mu\omega H_{y,n} \tag{14}$$

Now applying Poynting power theorem, the power dissipated per unit volume in each solid layer can be calculated as [25]:

$$\dot{Q}_n(x) = \frac{1}{2}\omega\varepsilon_0\varepsilon''_n|E_{z,n}|^2, \quad n = 1,\ldots,3 \tag{15}$$

It is important to note that the source term presented in Eq. (15) is a function of the temperature (T) and location (x). The temperature dependency comes from the dielectric properties such as dielectric loss and dielectric constant in the attenuation factor and the phase factor as well as in the transmission and reflection coefficients.

3.2. Energy equation and temperature distribution

The one dimensional energy equation subjected to electromagnetic heating can be simplified as

$$\alpha\frac{\partial^2 T(x,t)}{\partial x^2} + \frac{\alpha}{k}\dot{Q}(T,x) = \frac{\partial T(x,t)}{\partial t} \tag{16}$$

where α is the thermal diffusivity and k is the thermal conductivity. It is important to note that the governing Eq. (16) is nonlinear due to the temperature dependent source term. Hence, finding a close-form analytic expression for this system is not trivial. Recently our group [24] presented an algorithm to incorporate the nonlinear source term in determining the temperature distribution from energy equation. In that study it was assumed that for a short duration (Δt) of processing time ($t \to t + \Delta t$) the variation in dielectric properties will be negligible due to small changes in the temperature of the body. Thus, a close-form analytical expression was obtained for temperature distribution for a short period of processing time ($\Delta t \leqslant 1$ s), and that solution was used as the initial condition for the next time step. This procedure is continued until the final processing time has reached. This algorithm provided very accurate analytical solution of non-linear energy equation for radio frequency heating of food stuff [24]. In this study, a similar algorithm is adopted to solve the energy equation (Eq. (16)) for microwave assisted bonding process. Here our next step is to assume that the source term to be temperature independent for a short period of processing time (Δt) and then find a close-form analytical expression for temperature distribution for that period.

Thus, for the case of a multilayered solid shown in Fig. 1, Eq. (16) can be expressed as

$$\alpha_n\frac{\partial^2 T_n(x,t)}{\partial x^2} + \frac{\alpha_n}{k_n}\dot{Q}_n(x) = \frac{\partial T_n(x,t)}{\partial t} \quad \text{at } x_n \leqslant x \leqslant x_{n+1}, \quad n = 1,\ldots,3 \tag{17a}$$

where n denotes the layer number. The initial and boundary conditions for the multilayered system shown in Fig. 1 are:

$$-k_1\frac{\partial T_1}{\partial x} + h_1 T_1 = h_1 T_a \quad \text{at } x = x_1, \tag{17b}$$

$$\left.\begin{array}{l} T_n = T_{n+1} \\ k_n \frac{\partial T_n}{\partial x} = k_{n+1} \frac{\partial T_{n+1}}{\partial x} \end{array}\right\} \quad \text{at} \begin{array}{l} x = x_n \\ n = 2,3 \end{array} \tag{17c}$$

$$k_3 \frac{\partial T_3}{\partial x} + h_4 T_3 = h_4 T_b \quad \text{at } x = x_4 \tag{17d}$$

$$T_n = F_n, \quad n = 1,\ldots,3 \quad \text{at } t = t_i \tag{17e}$$

where T_a and T_b are the surrounding temperature at the layer boundaries $x = x_1$ and $x = x_4$, respectively. F_n is the temperature of the nth layer at initial time t_i.

The problem presented in Eq. (17) is transient heat conduction for three layered composite medium with temperature independent source term and non-homogenous outer boundary condition. This problem can be transformed into a one with homogenous boundary conditions by considering $T_n(x,t)$ as a linear superposition of three simpler problems as explained in Ref. [26],

$$T_n(x,t) = \phi_n(x) T_a + \psi_n(x) T_b + \theta_n(x,t), \quad n = 1,\ldots,3,\ x_n \leqslant x \leqslant x_{n+1};\ t > t_i \tag{18}$$

The functions $\phi_n(x)$ are the solution of the following steady-state problem with no heat generation and one non-homogenous boundary condition at $x = x_1$,

$$\frac{d}{dx}\left(\frac{d\phi_n}{dx}\right) = 0 \quad \text{in } x_n \leqslant x \leqslant x_{n+1};\ n = 1,\ldots,3 \tag{19a}$$

subject to boundary conditions

$$-k_1 \frac{d\phi_1}{dx} + h_1 \phi_1 = h_1 \quad \text{at } x = x_1 \tag{19b}$$

$$\left.\begin{array}{l} \phi_n = \phi_{n+1} \\ k_n \frac{d\phi_n}{dx} = k_{n+1} \frac{d\phi_{n+1}}{dx} \end{array}\right\} \quad \text{at} \begin{array}{l} x = x_{n+1} \\ n = 1,\ldots,2 \end{array} \tag{19c}$$

$$k_3 \frac{d\phi_3}{dx} + h_4 \phi_3 = 0 \quad \text{at } x = x_4 \tag{19d}$$

Similarly, the functions $\psi_n(x)$ are the solution of the following steady-state problem with no heat generation and one non-homogenous boundary condition at $x = x_4$,

$$\frac{d}{dx}\left(\frac{d\psi_n}{dx}\right) = 0 \quad \text{in } x_n \leqslant x \leqslant x_{n+1};\ n = 1,\ldots,3 \tag{20a}$$

subject to boundary conditions

$$-k_1 \frac{d\psi_1}{dx} + h_1 \psi_1 = 0 \quad \text{at } x = x_1 \tag{20b}$$

$$\left.\begin{array}{l} \psi_n = \psi_{n+1} \\ k_n \frac{d\psi_n}{dx} = k_{n+1} \frac{d\psi_{n+1}}{dx} \end{array}\right\} \quad \text{at} \begin{array}{l} x = x_{n+1} \\ n = 1,\ldots,2 \end{array} \tag{20c}$$

$$k_3 \frac{d\psi_3}{dx} + h_4 \psi_3 = h_4 \quad \text{at } x = x_4 \tag{20d}$$

Finally, the functions $\theta_n(x,t)$ are the solution of the following transient problem with heat generation and homogenous boundary conditions,

$$\alpha_n \frac{\partial^2 \theta_n(x,t)}{\partial x^2} + \frac{\alpha_n}{k_n} \dot{Q}_n(x) = \frac{\partial \theta_n(x,t)}{\partial t} \quad x_n \leqslant x \leqslant x_{n+1};\ n = 1,\ldots,3 \quad \text{for } t > t_i \tag{21a}$$

subject to boundary conditions at $t > t_i$

$$-k_1 \frac{\partial \theta_1}{\partial x} + h_1 \theta_1 = 0 \quad \text{at } x = x_1 \tag{21b}$$

$$\left.\begin{array}{l} \theta_n = \theta_{n+1} \\ k_n \frac{\partial \theta_n}{\partial x} = k_{n+1} \frac{\partial \theta_{n+1}}{\partial x} \end{array}\right\} \quad \text{at} \begin{array}{l} x = x_{n+1} \\ n = 1,\ldots,2 \end{array} \tag{21c}$$

$$k_3 \frac{\partial \theta_3}{\partial x} + h_4 \theta_3 = 0 \quad \text{at } x = x_4 \tag{21d}$$

and initial condition

$$\theta_n(x,t_i) = F_n - \phi_n(x) T_a - \psi_n(x) T_b = \overline{F}_n \quad \text{for } n = 1,\ldots,3 \tag{21e}$$

where $\overline{F}_n$ is the modified initial condition.

The solutions of steady state problems, shown in Eqs. (19) and (20), can be obtained as

$$\phi_1 = \frac{\frac{1}{h_4} + \frac{L_3}{k_3} + \frac{L_2}{k_2} + \frac{(x_2 - x)}{k_1}}{\left[\frac{L_1}{k_1} + \frac{1}{h_1} + \frac{1}{h_4} + \frac{L_2}{k_2} + \frac{L_3}{k_3}\right]} \tag{22a}$$

$$\phi_2 = \frac{\frac{1}{h_4} + \frac{L_3}{k_3} + \frac{(x_3 - x)}{k_2}}{\left[\frac{L_1}{k_1} + \frac{1}{h_1} + \frac{1}{h_4} + \frac{L_2}{k_2} + \frac{L_3}{k_3}\right]} \tag{22b}$$

$$\phi_3 = \frac{\frac{1}{h_4} + \frac{(x_4 - x)}{k_3}}{\left[\frac{L_1}{k_1} + \frac{1}{h_1} + \frac{1}{h_4} + \frac{L_2}{k_2} + \frac{L_3}{k_3}\right]} \tag{22c}$$

$$\psi_1 = \frac{\frac{1}{h_1} - \frac{(x_1 - x)}{k_1}}{\left[\frac{L_1}{k_1} + \frac{1}{h_1} + \frac{1}{h_4} + \frac{L_2}{k_2} + \frac{L_3}{k_3}\right]} \tag{23a}$$

$$\psi_2 = \frac{\frac{1}{h_1} + \frac{L_1}{k_1} - \frac{(x_2 - x)}{k_2}}{\left[\frac{L_1}{k_1} + \frac{1}{h_1} + \frac{1}{h_4} + \frac{L_2}{k_2} + \frac{L_3}{k_3}\right]} \tag{23b}$$

$$\psi_3 = \frac{\frac{1}{h_1} + \frac{L_1}{k_1} + \frac{L_2}{k_2} - \frac{(x_3 - x)}{k_3}}{\left[\frac{L_1}{k_1} + \frac{1}{h_1} + \frac{1}{h_4} + \frac{L_2}{k_2} + \frac{L_3}{k_3}\right]} \tag{23c}$$

On the other hand, the transient problem with heat generation term, given in Eq. (21), is solved using the Green's function approach. The general solution of this problem can be expressed in terms of Green's function as,

$$\theta_n(x,t) = \sum_{j=1}^{3} \left[\int_{x_j}^{x_{j+1}} G_{nj}(x,t|x',0) \overline{F}_j dx' + \int_{\tau=0}^{t} d\tau \int_{x_j}^{x_{j+1}} G_{nj}(x,t|x',\tau) \left[\frac{\alpha_j}{k_j} \dot{Q}_n(x')\right] dx' \right] \tag{24}$$

where $G_{nj}(x,t|x',0)$ represents the Green's function evaluated for $\tau = 0$ and $G_{nj}(x,t|x',\tau)$ represents the Green's function evaluated for $t = \tau$.

Our next step is to obtain the Green's function $G_{nj}(x,t|x',0)$. For $\tau = 0$, we consider an auxiliary problem by modifying Eq. (21) with $\dot{Q}_n(x) = 0$.

$$\alpha_n \frac{\partial^2 \theta_n(x,t)}{\partial x^2} = \frac{\partial \theta_n(x,t)}{\partial t} \quad x_n \leqslant x \leqslant x_{n+1};\ n = 1,\ldots,3 \tag{25a}$$

$$-k_1 \frac{\partial \theta_1}{\partial x} + h_1 \theta_1 = 0 \quad \text{at } x = x_1 \tag{25b}$$

$$\left.\begin{array}{l} \theta_n = \theta_{n+1} \\ k_n \frac{\partial \theta_n}{\partial x} = k_{n+1} \frac{\partial \theta_{n+1}}{\partial x} \end{array}\right\} \quad \text{at} \begin{array}{l} x = x_{n+1} \\ n = 1,\ldots,2 \end{array} \tag{25c}$$

$$k_3 \frac{\partial \theta_3}{\partial x} + h_4 \theta_3 = 0 \quad \text{at } x = x_4 \tag{25d}$$

and initial condition

$$\theta_n(x,t_i) = F_n - \phi_n(x) T_a - \psi_n(x) T_b = \overline{F}_n \quad \text{for } n = 1,\ldots,3 \tag{25e}$$

The partial derivatives of $\theta_n(x,t)$ with respect to x and t can be eliminated by the separation of variables technique. The variables can be separated in the form,

$$\theta_n(x,t) = \mathrm{X}_n(x) \Gamma_n(t) \tag{26}$$

Substitution of Eq. (26) into Eq. (25) and applying the appropriate boundary and initial conditions to solve for $X_n(x)$ and $\Gamma_n(t)$ respectively, we get the solution for the auxiliary problem as,

$$\theta_n(x,t) = \sum_{j=1}^{3} \int_{x'_j}^{x'_{j+1}} G_{nj}(x,t|x',0)\overline{F}_j dx' \tag{27}$$

where

$$G_{nj}(x,t|x',0) = \sum_{m=1}^{\infty} e^{-\lambda_m^2 t} \frac{1}{N_m} \frac{k_j}{\alpha_j} X_{nm}(x) X_{jm}(x')$$

$$N_m = \sum_{j=1}^{3} \frac{k_j}{\alpha_j} \int_{x_j}^{x_{j+1}} X_{jm}^2(x)dx$$

In the above solution, X_{nm} is obtained by solving the following eigenvalue problem,

$$\alpha_n \frac{d^2X_n(x)}{dx^2} + \lambda^2 X_n(x) = 0 \quad x_n \leqslant x \leqslant x_{n+1};\ n = 1,\ldots,3 \tag{28a}$$

$$-k_1 \frac{dX_1}{dx} + h_1 X_1 = 0 \quad \text{at } x = x_1 \tag{28b}$$

$$\left.\begin{array}{l} X_n = X_{n+1} \\ k_n \frac{dX_n}{dx} = k_{n+1} \frac{dX_{n+1}}{dx} \end{array}\right\} \quad \text{at} \quad \begin{array}{l} x = x_{n+1} \\ n = 1,\ldots,2 \end{array} \tag{28c}$$

$$k_3 \frac{dX_3}{dx} + h_4 X_3 = 0 \quad \text{at } x = x_4 \tag{28d}$$

The general solution for X_{nm} is expressed as

$$X_{nm} = A_{nm} \cos\left(\frac{\lambda_m x}{\sqrt{\alpha_n}}\right) + B_{nm} \sin\left(\frac{\lambda_m x}{\sqrt{\alpha_n}}\right), \quad n = 1,\ldots,3 \tag{29}$$

Now applying the boundary conditions, Eqs. (28b)–(28d), into Eq. (29) we obtain a set of six linear algebraic equations which can be used to find the coefficients and eigenvalues. The eigenvalues λ_m are obtained by the requirement that the determinant of the matrix formed from the above mentioned six algebraic equations should equal zero. Our next step is to find coefficients for the general solution (Eq. (29)). Since our system of equations is homogeneous with six unknown coefficients, it is not possible to get a trivial solution. Now by setting $A_{1m} = 1$, we can find remaining five coefficients using a set of any five algebraic equations by applying the matrix inversion technique [26].

Note that the solution for the auxiliary problem Eq. (27) does not include the source term $\dot{Q}_n(x)$. Hence, to include the contribution of the source term, it is required to find the Green's function $G_{nj}(x,t|x',\tau)$ evaluated at time $t = \tau$. The Green's function $G_{nj}(x,t|x',\tau)$ can be obtained from $G_{nj}(x,t|x',0)$ by replacing τ with $(t-\tau)$ in the latter as explained in Ref. [26].

$$G_{nj}(x,t|x',\tau) = \sum_{m=1}^{\infty} e^{-\lambda_m^2(t-\tau)} \frac{1}{N_m} \frac{k_j}{\alpha_j} X_{nm}(x) X_{jm}(x') \tag{30}$$

Now, to obtain the solution for problem defined in Eq. (21) it requires the substitution of Green's function $G_{nj}(x,t|x',0)$ and $G_{nj}(x,t|x',\tau)$ into the general solution (Eq. (24)). After rearranging the terms in the general solution, the solution for modified temperature (θ) of each solid layer is expressed as

$$\theta_n(x,t) = \sum_{m=1}^{\infty} \left[\begin{array}{l} \left(X_{nm}(x) e^{-\lambda_m^2 t} \frac{1}{N_m} \sum_{j=1}^{3} \frac{k_j}{\alpha_j} \int_{x_j}^{x_{j+1}} X_{jm}(x') \overline{F}_j dx' \right) + \\ \left(X_{nm}(x) \left(\int_{\tau=0}^{t} e^{-\lambda_m^2(t-\tau)} d\tau \right) \frac{1}{N_m} \sum_{j=1}^{3} \int_{x_j}^{x_{j+1}} X_{jm}(x') \dot{Q}_n(x') dx' \right) \end{array} \right], \quad n = 1,\ldots,3 \tag{31}$$

In Eq. (31) the subscript n denotes the n^{th} solid layer being considered and the subscript m denotes the Eigenvalue. Now we have expression for the three functions $\phi_n(x)$, $\psi_n(x)$ and $\theta_n(x,t)$ that are required to find the temperature distribution. By substitution of Eqs. (22), (23) and (31) into Eq. (18), the temperature distribution $T_n(x,t)$ within each solid layer due to microwave heating is obtained as

$$T_1(x,t) = \phi_1 T_a + \psi_1 T_b + \theta_1 \tag{32a}$$

$$T_2(x,t) = \phi_2 T_a + \psi_2 T_b + \theta_2 \tag{32b}$$

$$T_3(x,t) = \phi_3 T_a + \psi_3 T_b + \theta_3 \tag{32c}$$

The above expression for temperature is valid only for a short duration (Δt) of electromagnetic heating. To obtain the temperature distribution for a processing time of t_{total}, we need to solve Eq. (17a) for N times, where $N = t_{total}/\Delta t$. It is to be noted that the dielectric properties and initial condition for each time step will be calculated using the solution obtained from of the previous time step.

4. Results and discussion

The schematic representation of electromagnetic heating of three layered solid is shown in Fig. 1, where poly-aniline is sandwiched between two PMMA layers. Here our goal is to heat poly-aniline via microwave processing to above 105 °C, which is the glass transition temperature of PMMA. The volumetric heat generated in poly-aniline layer is transferred to PMMA by thermal conduction, and eventually heat is dissipated from PMMA surface to the surrounding by convection. The high temperature of poly-aniline results in localized melting of PMMA substrates close to the interface. The melted faces of PMMA will join together without any external force when the PMMA substrates will be allowed to cool down.

In this analysis the thickness of poly-aniline is maintained as low as possible to avoid the presence of interfacial layers after bonding. Throughout the analysis the incident radiation was maintained at 2.45 GHz due to the transparent nature of PMMA to microwave radiations at that frequency [15,16,18,19]. Close-form analytic expressions of electric field and temperature are obtained by considering transverse electromagnetic wave with temperature dependent dielectric properties. The algorithm used to take care of the temperature dependent dielectric properties are presented in Fig. 2. The relationship between dielectric properties and temperature are obtained from experimental data [16] using statistical regression, and are presented in Table 1. Other thermo-physical properties of PMMA and poly-aniline are also presented in Table 1, while the input parameters are shown in Table 2.

The temperature distribution obtained with analytical solution (in Eq. (32)) is validated with experimental data from Yussuf et al. [16]. Here we considered 4 mm thick PMMA layers ($L_1 = L_3 = 4$ mm), 300 μm thick Poly-aniline layer, and 12 W/cm^2 input power to match the experimental conditions used in Ref. [16]. Fig. 3 illustrates that the temperature distribution based on the current analytic solution which is in good qualitative agreement with the experimental results. The slight variation in temperature at or after 6 s is due to phase change of PMMA and poly-aniline at higher temperature. Here it is important to note that we did not consider the phase change effect in our analytic model. Rather, to simplify the mathematical model, the effect of phase change was taken into consideration through temperature dependent dielectric properties. Nevertheless, the difference in temperature is within the experimental uncertainty level validating the current method. We also presented the temperature distribution using the constant dielectric properties which deviates significantly from the experimental observation. These results suggest that the use of temperature dependent dielectric properties is

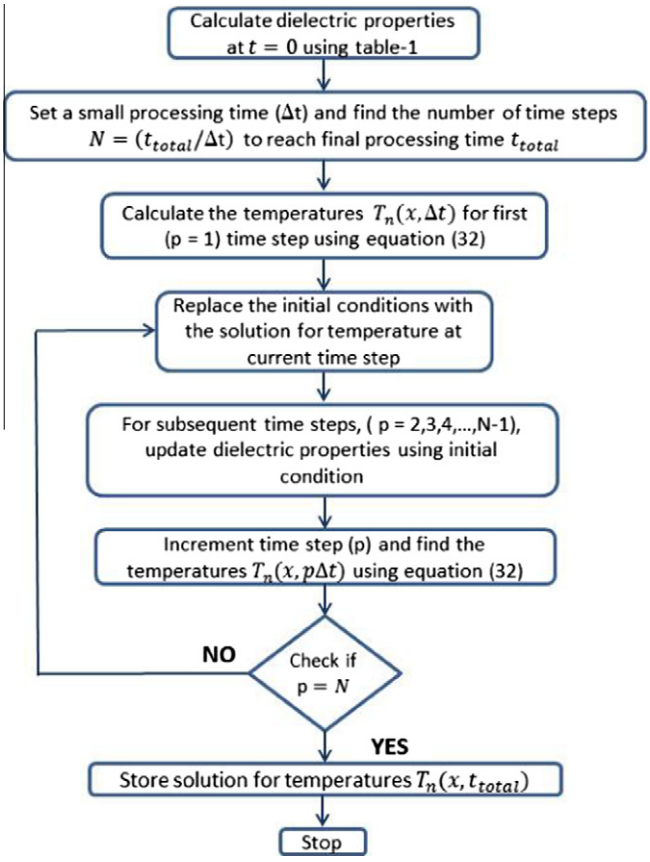

Fig. 2. Algorithm used to calculate temperature distribution within each layer using temperature dependent dielectric properties.

Table 1
Dielectric and thermo-physical properties of PMMA and poly-aniline.

	PMMA	Poly-aniline
Dielectric constant, k'	2.5	$-0.000003T^3 + 0.0003T^2 - 0.0078T + 14.56$
Dielectric loss, k''	0.05	For $T \leqslant 90$, $0.000001T^3 - 0.00004T^2 + 0.0126T + 3.6731$ For $T \geqslant 91$, $-0.0005T^2 + 0.1037T - 0.0629$
Specific heat capacity, c_P (J/kg K)	1200	1100
Thermal conductivity, k (W/m K)	0.1	1
Density, ρ (kg/m^3)	1300	1700

Table 2
Input parameters for theoretical calculations.

Parameters	Values
Incident microwave frequency	2450 MHz
Thickness of PMMA, L_1, L_3 (mm)	3 or 4
Thickness of Poly-aniline, L_2 (μm)	100, 150, 200, 250
Initial Temperature, T_i (°C)	20
Surrounding temperature, T_∞ (°C)	20
Heat transfer coefficient, h (W/m^2 K)	1.5, 10, 25, 50
Incident microwave energy flux, $I_T = I_B$ (W/cm^2)	3.0 and 12

much better in predicting the thermal performance during microwave heating process.

For the rest of the article, analytic results are obtained for temperature dependent dielectric properties, and the incidence microwave energy flux ($I_T = 0.5c\varepsilon_0 E^2$) was kept constant at 3 W/cm^2. Moreover, it is assumed that the microwave radiations are coming

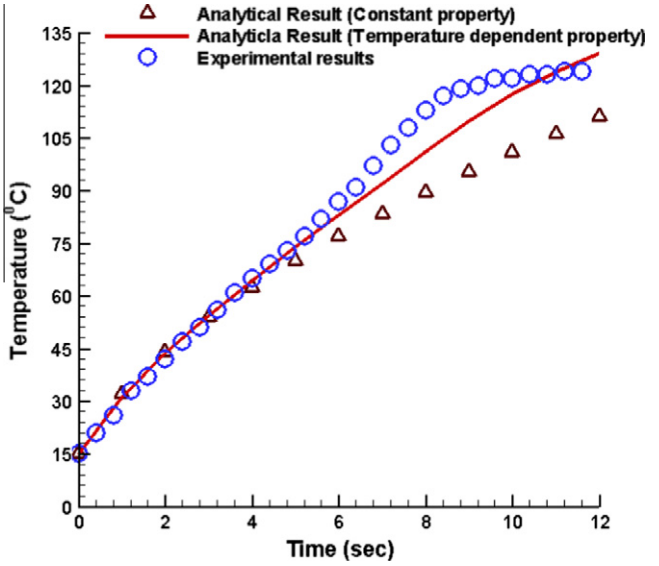

Fig. 3. Comparison of analytical solution with experimental data (Yussuf et. al. [15]). Temperature of poly-aniline layer is shown for various exposure time of electromagnetic radiation. Here thickness of PMMA layers (L_1 and L_3) is 4 mm, thickness of poly-aniline (L_2) is 300 μm and $I_T = 12$ W/cm^2.

from both directions as presented in Fig. 1. Due to the symmetry of layer materials, the electric field, microwave energy and temperature distribution are presented for only one half of the system.

The electric field and volumetric power distribution along wave propagation direction are presented in Fig. 4 for different thicknesses of intermediate poly-aniline layer. For convenience of comparison, the electric field and volumetric power distribution for each case is plotted against the normalized length where $x/L_1 = 0$ denotes the face where the outer PMMA surface reject heat to ambient air via convection, and $x/L_1 = 1$ represents the interface between the PMMA and the intermediate poly-aniline layer. The results obtained from the multi-layer analysis show continuity in electric field (Fig. 4(a)) at the interfaces to maintain the interface boundary conditions in the Maxwell's equation. However, there is a jump in volumetric heat generation (Fig. 4(b)) at the interface due to the use of different materials property in calculating the heat dissipation. As presented in Eq. (15), the volumetric power greatly depends on the dielectric property of the material. The dielectric loss value which is a measure of the electrical energy dissipation into heat primarily attributes to the difference in volumetric power absorbed by poly-aniline and PMMA. The huge difference in the source term would facilitate the selective and localized heating of poly-aniline when exposed to microwave radiation.

The thickness of poly-aniline also influences the electric field distribution in the PMMA substrate. Poly-aniline being highly dielectric absorbed much higher electromagnetic energy and resulted in higher electric field strength compared to the PMMA layer. It is also noteworthy to mention that the magnitude of electric field decreases as the thickness of the intermediate poly-aniline layer increases. This decrease in electric field strength is mainly due to the fact that the intensity of the incident field decays at a higher rate when it penetrates through samples of increased thickness. To validate the analytic model presented in this study, results are also obtained for multi-layered materials (not shown here) where all three layers consist of PMMA materials. These results match well with previous studies [20,21] where one layer of PMMA is used instead of three layers.

The volumetric power generated by each layer is used as a source term in solving the energy equation as expressed in Eq. (17a). Hence, the power distribution in each layer primarily

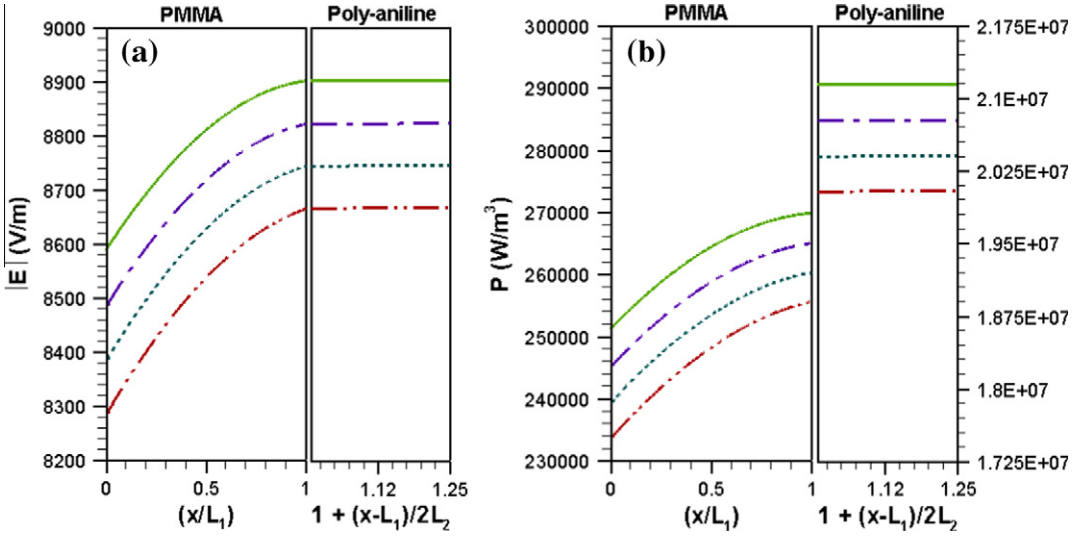

Fig. 4. (a) Electric field and (b) volumetric power distribution after 1 s processing of PMMA-poly-aniline-PMMA layers. Here the thickness of outer PMMA layers (L_1 and L_3) is 3 mm and I_T = 3 W/cm^2. The thicknesses of intermediate poly-aniline layer are: for L_2 = 100 μm, for L_2 = 150 μm, for L_2= 200 μm, for L_2 = 250 μm.

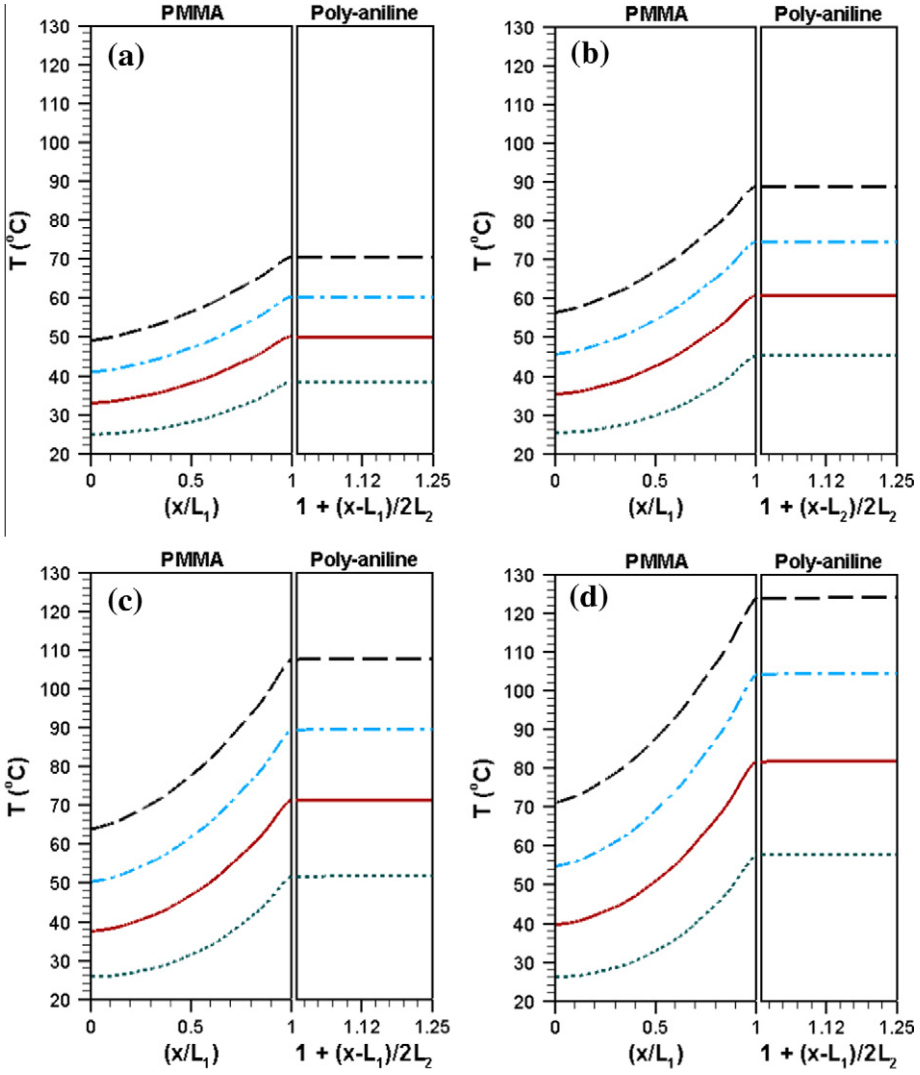

Fig. 5. The temperature distribution (at t = 25 s, at t = 50 s, at t = 75 s and at t = 100 s) in PMMA and poly-aniline layers for various thicknesses of poly-aniline. (a) L_2 = 100 μm (b) L_2 = 150 μm (c) L_2 = 200 μm and (d) L_2= 250 μm. Here the thickness of PMMA (L_1 and L_3) is 3 mm, I_T = 3 W/cm^2 and h = 10 W/m^2 K.

dictates the microwave heating and resultant temperature distribution. Fig. 5 present the temperature distribution in PMMA and poly-aniline for increasing poly-aniline thickness. In all cases, PMMA thickness was kept constant at 3 mm and the temperature distribution was analyzed for a processing time of t_{total} = 100 s. It was observed that temperature distribution qualitatively followed the volumetric power generation profile. The use of highly dielectric poly-aniline layer resulted in high temperatures close to the layer interface. Theoretical results show that the poly-aniline thickness as well as processing time significantly affects the temperature distribution. The maximum temperature in the system increases with the thickness of the poly-aniline layer, although volumetric power generation has shown the opposite trend. This is due to the fact that the thicker poly-aniline layer is producing more total heat in the system than that of a thinner one. After 100 s of exposure to electromagnetic radiation, the interface temperatures were 70 °C, 89 °C, 107 °C and 124 °C for 100 μm, 150 μm, 200 μm and 250 μm thick poly-aniline layers, respectively. Similar to the power profile, the temperature of poly-aniline was almost uniform because of the much smaller size and higher thermal conductivity than surrounding PMMA layer. It is noteworthy to mention that 100 μm, 150 μm and 200 μm thick poly-aniline layers required more exposure time to increase the interface temperature above the glass transition temperature of PMMA.

The high temperature of intermediate poly-aniline layer also influences the temperature distribution in the PMMA layer. At the interface the PMMA temperature is same as the poly-aniline, but temperature changes sharply along the PMMA layer due to its low thermal conductivity. The sharp temperature change facilitates the localized melting of PMMA close to the interface while a major portion of PMMA remains much below its glass transition temperature. For the case of 200 μm thick poly-aniline layer presented in Fig. 5c, PMMA temperature remains above its glass transition temperature (105 °C) only close to the layer interface, and reduces sharply thereafter. The analytical expression also indicates that the temperature distribution in both layers is greatly influenced by the PMMA thickness and the heat transfer coefficient. In the following sections we discuss the role of PMMA thickness and heat transfer coefficient on temperature distribution.

The effect of PMMA thickness on temperature distribution was analyzed and presented in Fig. 6. In this case, the PMMA thickness was maintained at 4 mm, while the poly-aniline thickness was varied like cases presented in Fig. 5. The thermal analysis was carried out for a processing time of t_{total} = 100 s. Here all other parameters such as frequency, dielectric properties, input power and heat

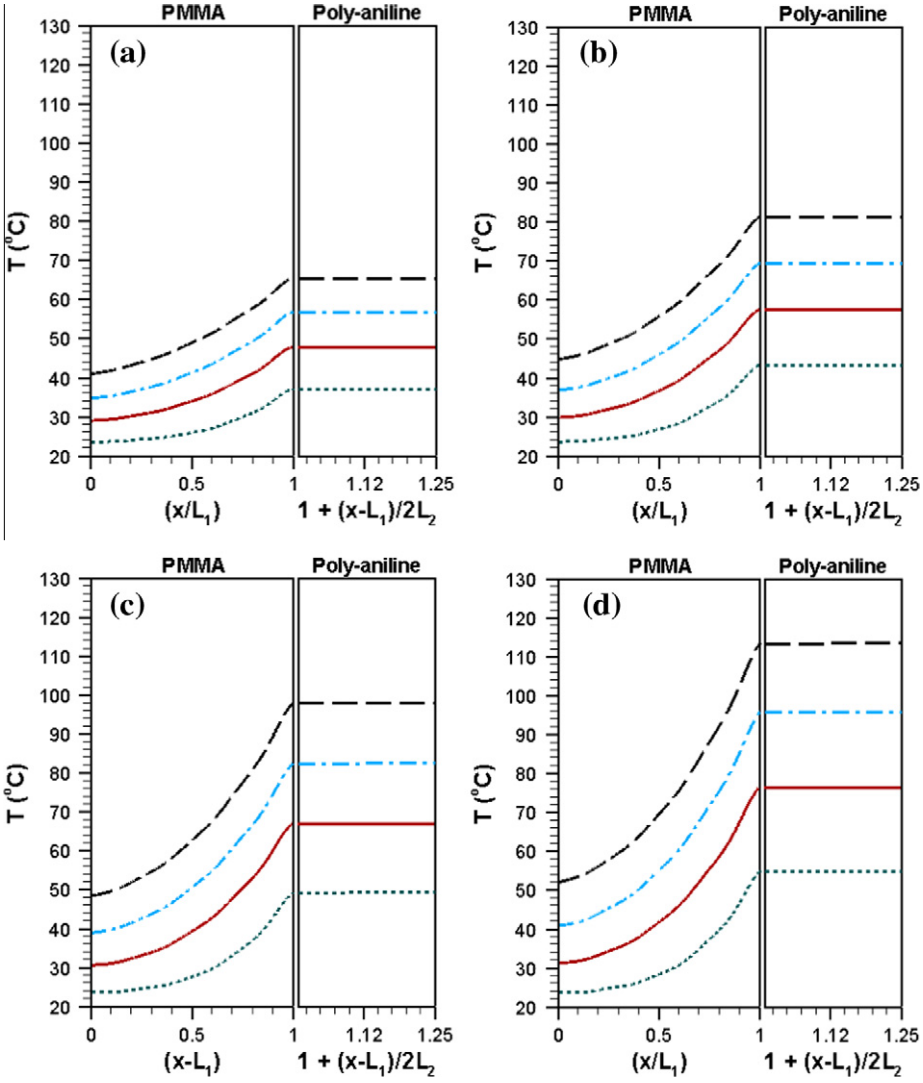

Fig. 6. The temperature distribution (at t = 25 s, at t = 50 s, at t = 75 s and at t = 100 s) in PMMA and poly-aniline layers for various thicknesses of poly-aniline. (a) L_2 = 100 μm (b) L_2= 150 μm (c) L_2 = 200 μm and (d) L_2 = 250μm. Here the thickness of PMMA (L_1 and L_3) is 4 mm, I_T = 3 W/cm^2 and h = 10 W/m^2 K.

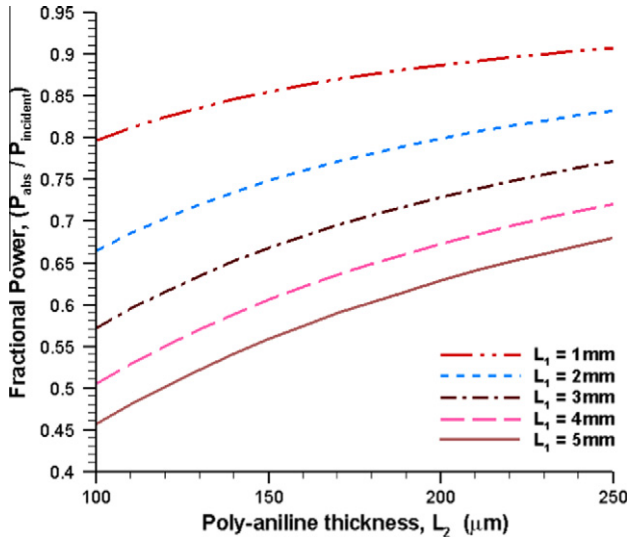

Fig. 7. The fractional power absorbed by poly-aniline for various thickness of poly-aniline layers (L_2) after 1 s of processing time. Here f = 2450 MHz and I_T = 3 W/cm^2.

transfer coefficient were kept same as in Fig. 5. For all cases, the temperature results (Fig. 6) showed a slight decrease when compared to the previous cases (Fig. 5) where the thickness of PMMA layer was 3 mm. For instance, at 100 s processing time, the interface temperatures were 65 °C, 81 °C, 98 °C, and 113 °C for 100 μm, 150 μm, 200 μm and 250 μm thick poly-aniline layer, respectively. However, there was no change in the pattern of heat flow in either PMMA or poly-aniline layers. Since an increase in the PMMA thickness would decrease the interface temperature, more exposure time is needed to achieve the desired temperature for bonding of two PMMA layers. In other words, exposure time should be higher for thicker PMMA substrates.

During microwave heating, the total power absorbed primarily dictates the temperature of the material. So in order to understand the drop in interface temperature for increased PMMA thickness, it is necessary to analyze the total power absorbed by poly-aniline. The power absorbed (P_{abs}) by each layer was obtained by integrating Eq. (11) over the thickness of the layer. From the power absorbed by each layer, the fractional power absorbed (which ranges from 0 to 1) by each layer were obtained. In Fig. 7 we present the fractional power absorbed by poly-aniline for different thicknesses of PMMA after 1 s of microwave processing. The

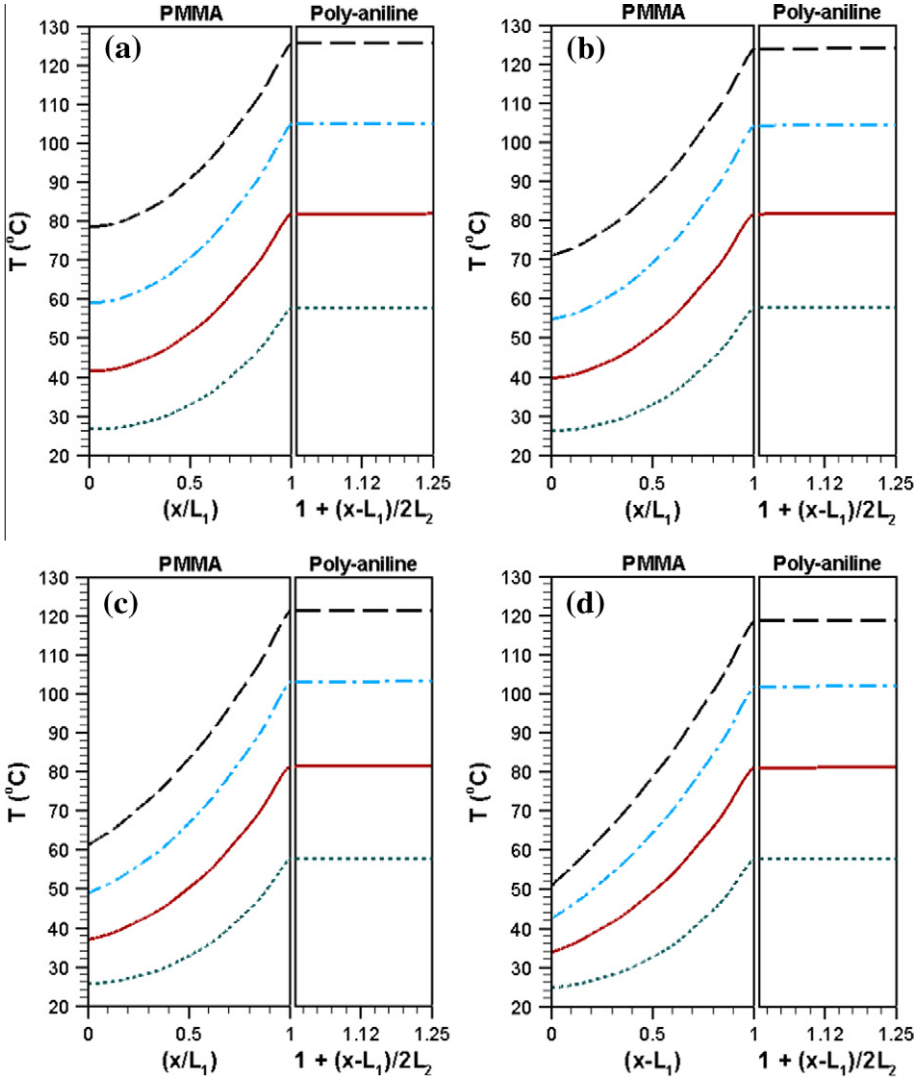

Fig. 8. The temperature distribution (▪▪▪▪ at t = 25 s, ——— at t = 50 s, —·— at t = 75 s and – – – – at t = 100 s) in PMMA and poly-aniline layers for various heat transfer coefficients. (a) h = 1.5 W/m^2 K (b) h = 10 W/m^2 K (c) h = 25 W/m^2 K and (d) h = 50 W/m^2 K. All other parameters are same as in Fig. 5.

fractional power is illustrated for various thicknesses of poly-aniline layers. It is interesting to note that the fractional power absorbed by poly-aniline was greatly influenced by the thickness of PMMA. For thick layers of PMMA, the fractional power absorbed by poly-aniline was low and it resulted in low interface temperatures.

We also investigated the effect of heat transfer coefficient during microwave heating of PMMA-poly-aniline-PMMA layers. This analysis was carried out for 3 mm thick PMMA layers and 250 μm thick poly-aniline layer while keeping all other input parameters same as in Fig. 5. Results show that the heat transfer coefficient has significant influence on the heat flow pattern inside PMMA layer. It was observed that after 100 s of exposure time the interface temperature remained above 120 °C for all cases, while the temperature at the outer boundary dropped by 30 °C for increase in heat transfer coefficient from 1.5 to 50 W/m^2 K. The drop in outer boundary temperature greatly changes the temperature distribution inside PMMA layer. During bonding process it is necessary to ensure that only a small portion of the PMMA layer (close to the interfaces) maintains the glass transition temperature, while a major portion remains at lower temperatures. This is to ensure that, the heat transfer process through PMMA does not affect the patterned micro channel. Our results show that by varying the heat transfer coefficient it was possible to control the region of PMMA layer (close to the interface) that can retains the glass transition temperature (105 °C). For high heat transfer coefficient value, as presented in Fig. 8d, the localized melting of PMMA occurs only for a short distance from the layer interface while leaving a major portion much below the glass transition temperature. It is also noteworthy to mention that the temperature difference between outer boundary of PMMA and the PMMA-poly-aniline interface tends to increases with high heat transfer coefficient values. Therefore, it is very much necessary to control the heat transfer rate at the outer boundaries to achieve a precise melting of the PMMA substrate only at the interface.

5. Summary and conclusions

Closed form analytical solutions are obtained for power and temperature distribution in PMMA and poly-aniline under microwave heating. The electromagnetic heat generation is obtained from Maxwell's equation using temperature dependent dielectric properties which is then used in the energy equation to find the temperature distribution. The temperature distribution is presented as a function of poly-aniline thickness, PMMA thickness and heat transfer coefficient for various microwave exposure time. This study results in following conclusions.

1. The power and temperature distribution in the sample reveals that the highly dielectric poly-aniline absorbed more microwave power and resulted in high temperatures compared to PMMA.
2. Due to the Low thermal conductivity, PMMA retained its glass transition temperature close to the interface and favors a localized melting.
3. The interface temperature rises with an increase in the thickness of poly-aniline. With 250 μm thick poly-aniline layer and 3 mm thick PMMA layer, it is possible to increase the interface temperature much above 105 °C (glass transition temperature of PMMA). Whereas for thin layers of poly-aniline, more processing time (exposure to microwave radiation longer than 100 s) is required.
4. For thick sample of PMMA, the fractional power absorbed by poly-aniline decreases, and more microwave exposure time is required to rise the interface temperature above 105 °C.
5. It is possible to obtain elevated temperatures at the layer interface either by increasing the poly-aniline thickness or by decreasing the thickness of PMMA.
6. Along with PMMA and poly-aniline thickness, the heat transfer coefficient at the outer boundaries also plays a major role in the temperature and heat flow pattern inside PMMA.
7. By varying the heat transfer coefficient it is also possible to control the temperature distribution inside PMMA layer as well as the distance up to which localized melting occurs. With high heat transfer coefficient at the outer boundaries one can achieve a precise and localized melting of PMMA without affecting a major portion of it.

References

[1] D.R. Reyes, D. Lossifidis, P. Auroux, Micro total analysis systems. I. Introduction, theory, and technology, Anal. Chem. 74 (2002) 2623–2636.
[2] G. Lee, S. Chen, G. Huang, W. Sung, Y. Lin, Micro fabricated plastic chips by hot embossing methods and their applications for DNA separation and detection, Sens. Actuators B 75 (2000) 142–148.
[3] L.J. Kricka, Miniaturization of analytical systems, Clin. Chem. 44 (1998) 2008–2014.
[4] P. Lidstorm, J. Tierney, B. Wathey, J. Westman, Microwave assisted organic synthesis – a review, Tetrahedron 57 (2001) 9225–9238.
[5] B.H. Weigl, R.L. Bardell, C.R. Cabrera, Lab-on-a-chip for drug development, Adv. Drug Delivery Rev. 55 (2003) 349–377.
[6] R.H. Liu, J. Yang, R. Lenigk, J. Bonanno, P. Grodzinski, Self-contained, fully integrated biochip for sample preparation, polymerase chain reaction amplification and DNA microarray detection, Anal. Chem. 76 (2004) 1824–1831.
[7] J. Wang, Microchip devices for detecting terrorist weapons, Anal. Chim. Act 507 (2004) 3–10.
[8] T.Z. Jubery, M.R. Hossan, D.R. Bottenus, C.F. Ivory, W. Dong, P. Dutta, A new fabrication technique to form complex Polymethylmethacrylate microchannel for bioseparation, Biomicrofludics 6 (2012) 016503.
[9] D. Bottenus, T.Z. Jubery, P. Dutta, C.F. Ivory, 10 000-fold concentration increase in proteins in a cascade microchip using anionic ITP by a 3-D numerical simulation with experimental results, Electrophoresis 32 (2011) 550–562.
[10] G.J. Cheng, D. Pirzada, P. Dutta, Design and fabrication of a hybrid nanofluidic channel, J. Microlithog. Microfab. Microsyst. 4 (2005) 013009.
[11] B. Bilenberg, T. Nielsen, B. Clausen, A. Kristensen, PMMA to SU-8 bonding for polymer based lab-on-chip systems with integrated optics, J. Micromech. Microeng. 14 (2004) 814–818.
[12] Y. Sun, Y.C. Kwok, N. Nguyen, Low-pressure, high-temperature thermal bonding of polymeric microfluidic devices and their applications for electrophoretic separation, J. Micromech. Microeng. 16 (2006) 1681–1688.
[13] C. Lin, C. Choa, C. Lan, Low azeotropic solvent for bonding of PMMA microfluidic devices, Sens. Actuators B 121 (2007) 698–705.
[14] S. Lai, X. Cao, J. Lee, A packaging technique for polymer microfluidic platforms, Am. Chem. Soc. Anal. Chem. 76 (2004) 1175–1183.
[15] K.F. Lei, S. Ahsan, N. Budraa, W.J. Li, J.D. Mai, Microwave bonding of polymer-based substrate for potential encapsulated micro/nanofluidic device fabrication, Sens. Actuators A 114 (2004) 340–346.
[16] A.A. Yussuf, I. Sbarski, J.P. Hayes, M. Solomon, N. Tran, Microwave welding of polymeric-microfludic devices, J. Micromech. Microeng. 15 (2005) 1692–1699.
[17] M. Rahbar, S. Chhina, D. Sameoto, M. Parameswarn, Microwave-induced, thermally assisted solvent bonding for low-cost PMMA microfluidic devices, J. Micromech. Microeng. 20 (2010) 15–26.
[18] A.A. Yussuf, I. Sbarski, M. Solomon, N. Tran, J.P. Hayes, Sealing of polymeric-microfluidic devices by using high frequency electromagnetic field and screen printing technique, J. Micromech. Microeng. 189 (2007) 401–408.
[19] R.J. Holmes, C. McDonagh, J.A.D. McLaughlin, S. Mohr, N.J. Goddard, P.R. Fielden, Microwave bonding of poly(methyl methacrylate) microfluidic devices using a conductive polymer, J. Phys. Chem. Solids 72 (2011) 626–629.
[20] G.J. Fleischman, Predicting temperature range in food slabs undergoing short-term/high power microwave heating, J. Food Eng. 40 (1998) 81–88.
[21] M.R. Hossan, D. Byun, P. Dutta, Analysis of microwave heating for cylindrical shaped objects, Int. J. Heat Mass Transfer 53 (2010) 5129–5138.
[22] T. Basak, Role of metallic, ceramic and composite plates on microwave processing of composite dielectric materials, Mater. Sci. Eng. A 457 (2007) 261–274.
[23] K.G. Ayappa, H.T. Davis, Microwave heating: an evaluation of power formulations, Chem. Eng. Sci. 46 (1991) 1005–1016.
[24] M.R. Hossan, P. Dutta, Effects of temperature dependent properties in electromagnetic heating, Int. J. Heat Mass Transfer 55 (2012) 3412–3422.
[25] G. Roussy, J.A. Pearce, Foundations and Industrial Applications of Microwaves and Radio Frequency Fields – Physical And Chemical Processes, John Wiley and Sons Ltd., West Sussex, England, 1995. pp. 7–25.
[26] M.N. Ozisik, Heat Conduction, second ed., John Wiley and Sons Ltd., New York, 1993.